Chemical Engineering Journal 106 (2005) 35–42

Chemical Engineering Journal

www.elsevier.com/locate/cej

Oxygen transport through LSM/YSZ/LaAlO system for use of fuel cell type reactor

Worapon Kiatkittipong[b,1], Tomohiko Tagawa[a,*], Shigeo Goto[a], Suttichai Assabumrungrat[b], Piyasan Praserthdam[b]

[a] *Department of Chemical Engineering, Nagoya University, Chikusa, Nagoya 464-8603, Japan*
[b] *Center of Excellence on Catalysis and Catalytic Reaction Engineering, Department of Chemical Engineering, Chulalongkorn University, Bangkok 10330, Thailand*

Received 29 September 2004; received in revised form 11 October 2004; accepted 3 November 2004

Abstract

Oxygen transport in an LSM/YSZ/LaAlO solid oxide fuel cell type reactor was studied. The oxygen permeation flux was 8.90×10^{-8} mol m^{-2} s^{-1} at 1173 K with an activation energy of 170 kJ mol^{-1}. By applying an external potential, the oxygen permeation flux increased while the activation energy of oxygen permeation decreased. The oxygen permeation fluxes under methane feed in the anode side are 1–2 orders of magnitude higher than those under helium feed. A model of oxygen permeation was presented and the permeation parameters were proposed. In the case of helium feed, the oxygen permeation at the LaAlO anode was the rate-limiting step. However, changing helium to methane as a reactive gas, the resistances for the oxygen permeation in the three parts (LSM/YSZ/LaAlO) were comparable.

Keywords: Solid oxide fuel cell; SOFC reactor; Oxygen permeation; Modeling; Methane

1. Introduction

Solid oxide fuel cell (SOFC) is a promising energy conversion technology for future applications [1,2]. In our previous papers, the SOFC system was applied as a selective oxidation reactor for chemical energy co-generation. Particular focuses were on catalyst preparation method [3–5] and reactor performance test [6–8]. In these studies, the oxidative coupling of methane to ethane and ethylene (C2) was studied. The solid electrolyte was used as an oxygen separator and an oxygen distributor to achieve high C2 selectivity. In these electrocatalytic systems, combined effects of activation of oxygen on an anode and permeation of oxygen through an yttria stabilized zirconia (YSZ) controlled the reactor performance.

Therefore, the oxygen transport through the electrochemical system should be studied. Several research groups have published their experimental results on the overall oxygen permeation through many oxygen-permeable electrolyte membranes such as YSZ [9], calcia stabilized zirconia (CSZ) [10], mixed ion-electronic conducting materials such as $La_{1-x}Sr_xCo_{1-y}Fe_yO_{3-\delta}$ (LSCF) [11,12] and other perovskite-type ceramics, for example, $Bi_{1.5}Y_{0.3}Sm_{0.2}O_{3-\delta}$ (BYS) [13,14], $BaBi_xCo_{0.2}Fe_{0.8-x}O_{3-\delta}$ [15], $BaCo_{0.4}Fe_{0.6-x}Zr_xO_{3-\delta}$ [16].

Several studies focused on the steady-state oxygen permeation in membrane reactors for oxidation reactions, for example, partial oxidation of methane [17] and oxidative coupling of methane [14,18]. However, very limited studies on oxygen permeation in the SOFC reactors have been reported. The conventional YSZ electrolyte has been widely used to provide the electrochemical permeation of oxygen for the oxidative coupling of methane [3–8]. The use of external potential as well as the effect of non-Faradaic electrochemical modification of catalytic activity (NEMCA) are of recent interest.

* Corresponding author. Tel.: +81 52 789 3388; fax: +81 52 789 3388.
E-mail address: tagawa@nuce.nagoya-u.ac.jp (T. Tagawa).
[1] Nagoya University Program for Academic Exchange (NUPACE)-Ph.D. student supported by AIEJ.

1385-8947/$ – see front matter © 2004 Elsevier B.V. All rights reserved.
doi:10.1016/j.cej.2004.11.004

Nomenclature

A_j	pre-exponential factor of conductivity ($S\,K\,m^{-1}$)
A_{Per}	pre-exponential factor of oxygen permeation ($mol\,m^{-2}\,s^{-1}$)
E	electromotive force (V)
E_j	activation energy of conductivity ($J\,mol^{-1}$)
E_{Per}	activation energy of oxygen permeation ($J\,mol^{-1}$)
F	Faraday's constant, 96487 ($C\,mol^{-1}$)
J_{O_2}	oxygen permeation flux ($mol\,m^{-2}\,s^{-1}$)
$k_{O_2\text{-perm}}$	overall oxygen ions recombination and diffusion coefficient ($mol\,m^{-2}\,s^{-1}$)
$k_{O_2\text{-Rxn}}$	oxygen surface reaction coefficient ($mol\,m^{-2}\,s^{-1}\,Pa^{-1}$)
k_V	proportional constant ($mol\,m^{-2}\,s^{-1}\,V^{-1}$)
L	thickness of material (m)
Per, O	specific oxygen permeability ($mol\,m^{-1}\,s^{-1}$)
P_{feed}	oxygen partial pressure at feed side (cathode side) (Pa)
P_{lean}	oxygen partial pressure at lean side of materials (Pa)
$P_{O_2(I)}$	oxygen partial pressure at the gas–membrane interface (Pa)
$P_{O_2(II)}$	oxygen partial pressure at membrane–gas interface (Pa)
P_{perm}	oxygen partial pressure at permeate side (anode side) (Pa)
P_{rich}	oxygen partial pressure at rich side of materials (Pa)
R_g	gas constant, 8.314 ($J\,mol^{-1}\,K^{-1}$)
T	temperature (K)
V_{Per}	applied external potential during steady-state permeation (V)

Greek letters

α	permeation rate constants in interface diffusion step ($mol\,m^{-2}\,s^{-1}\,Pa^{-1/2}$)
β	permeation rate constants in bulk diffusion step ($mol\,m^{-1}\,s^{-1}\,Pa^{-1/4}$)
σ	conductivities ($S\,m^{-1}$)

Subscripts

e	electronic
i	ionic

In the previous paper [8], the fuel cell type temperature-programmed desorption (FC-TPD) was studied on the LSM/YSZ/LaAlO system. Increasing the applied potential increased the amount of adsorbed oxygen. The change in the selectivity of active sites gave a new aspect to the NEMCA phenomena in the oxidative coupling of methane in the SOFC reactor. The applied potential also decreased the activation energy of desorption of oxygen at the anode catalyst [19]. In addition, the FC-TPD analysis could correlate the behavior of adsorbed oxygen species to the NEMCA effect.

In this study, the steady-state oxygen permeation using helium or methane as an anode gas was investigated. The effect of applied potential on the oxygen permeation through the LSM/YSZ/LaAlO in the SOFC reactor was studied. In addition, a model of oxygen permeation was proposed.

2. Experimental

2.1. Apparatus

The schematic diagram of the solid oxide fuel cell type reactor is illustrated in Fig. 1. A tube-type YSZ membrane (8 mol% Y_2O_3, thickness = 1.5 mm, inside diameter = 18 mm, outside diameter = 21 mm, length = 500 mm, effective surface area = 0.0148 m^2) was used as an electrolyte. $La_{1.8}Al_{0.2}O_3$ (abbreviated as LaAlO) prepared by a mist decomposition method was used as an anode catalyst on the inner surface of the tube while $La_{0.85}Sr_{0.15}MnO_3$ (abbreviated as LSM) prepared by paste method was used as the cathode on the outer surface [7,8]. Details of the electrode preparation methods were described elsewhere [3,4,7].

Platinum wire was connected to platinum meshes placed on both electrode surfaces to serve as current collectors. The outlet gas from the anode side was directly connected to a gas chromatograph for analysis of gas composition. A potentiostat was used to supply an external electrical potential to the system. Oxygen transport from the cathode side to the anode side was promoted under the applied positive potential.

2.2. Steady-state oxygen permeation

Steady-state oxygen permeation measurements were performed at various temperature levels: i.e., T = 1073, 1123, 1173, 1223 and 1273 K. Helium (1.36×10^{-5} mol s^{-1}) and oxygen (1.02×10^{-5} mol s^{-1}) were fed to the anode and the cathode, respectively. The oxygen permeation flux was calculated from the flow rate and composition of the anode exit gas. The flow rate and its composition was measured and analyzed by a bubble flow meter and a gas chromatograph with a TCD detector, respectively. Sampling was conducted every 5 min until reaching a steady-state condition (approximately 0.5 h). Another set of steady-state oxygen permeation was carried out by using methane (6.8×10^{-6} mol s^{-1}) as an anode reactant gas at various temperature levels: i.e. T = 1073, 1123, 1173, 1223 and 1273 K. In this case, permeated oxygen has reacted with methane to produce oxygen, containing species such as CO, CO_2, H_2O. Thus, the oxygen permeation flux was estimated by analyzing these oxygen-containing products. The steady-state measurements for both sets of experiments were carried out at various levels of the applied potential.

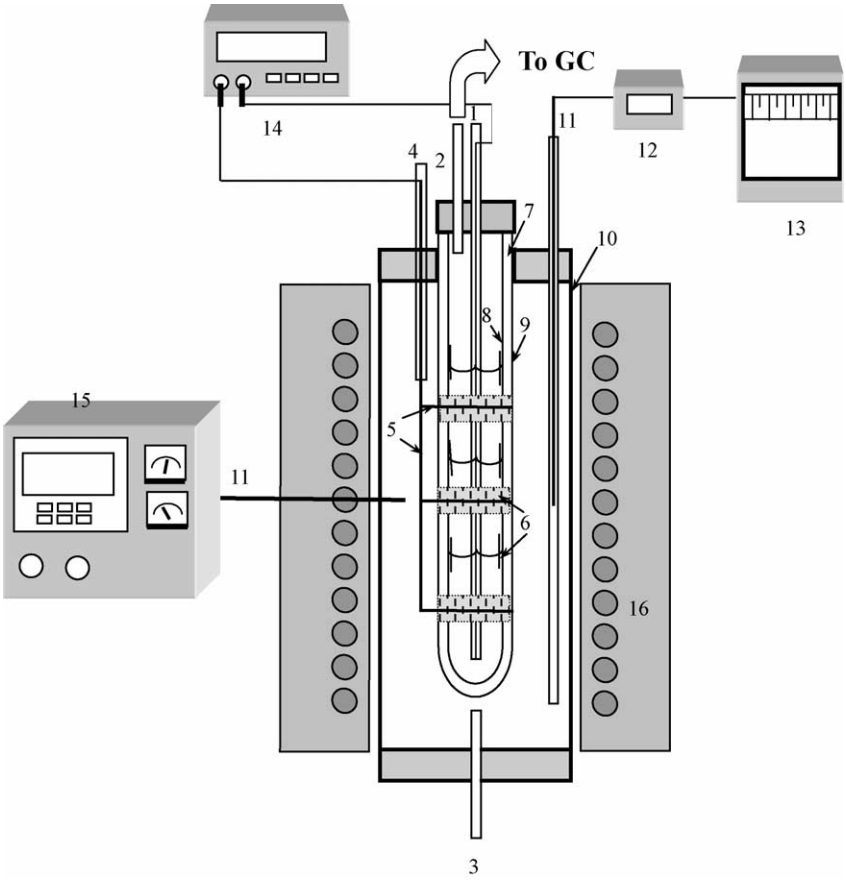

Fig. 1. Schematic diagram of the solid oxide fuel cell type reactor. (1) Anode side feed (He/CH_4), (2) exit gas from anode side, (3) cathode side feed (O_2), (4) exit gas from cathode side, (5) platinum wire, (6) platinum mesh, (7) YSZ tube, (8) anode (LaAlO), (9) cathode (LSM), (10) quartz tube, (11) thermocouple, (12) temperature indicator, (13) temperature recorder, (14) ammeter/voltmeter/potentiostat, (15) temperature controller, (16) furnace.

3. Results and discussion

3.1. Oxygen transport model

3.1.1. Oxygen permeation through thin YSZ membranes modeled by Han et al. [9]

In our previous study on the micro fuel cell system [20], we have referred an oxygen permeation model presented by Han et al. [9]. The proposed permeation process is summarized in Fig. 2. In their study, a thin YSZ membrane prepared by the electrochemical vapor deposition (EVD) method was employed. The oxygen permeation flux can be described by the following equations [9].

At gas-membrane interface of the cathode side:

$$J_{O_2} = \alpha(P_{\text{rich}}^{1/2} - P_{O_2(I)}^{1/2}) \quad (1)$$

In bulk oxide of YSZ:

$$J_{O_2} = \frac{\beta}{L}(P_{O_2(I)}^{1/4} - P_{O_2(II)}^{1/4}) \quad (2)$$

At membrane–gas interface of the anode side:

$$J_{O_2} = \alpha(P_{O_2(II)}^{1/2} - P_{\text{lean}}^{1/2}) \quad (3)$$

The rate parameters α and β at $T = 1173\,K$ are $9.4 \times 10^{-7}\,\text{mol}\,m^{-2}\,s^{-1}\,Pa^{-1/2}$ and $5.2 \times 10^{-11}\,\text{mol}\,m^{-1}\,s^{-1}\,Pa^{-1/4}$, respectively. The activation energy of α and β are $53.1\,\text{kJ}\,\text{mol}^{-1}\,K^{-1}$ and $72.0\,\text{kJ}\,\text{mol}^{-1}\,K^{-1}$, respectively. As

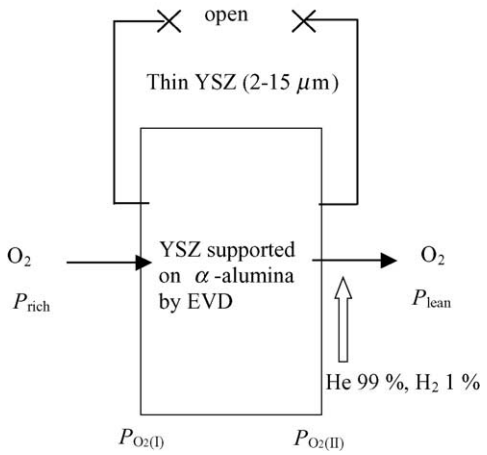

Fig. 2. Oxygen permeation process through thin YSZ membranes prepared by the electrochemical vapor deposition (EVD) method supported on α-alumina reported by Han et al. [9].

shown in Fig. 2, this system was operated under open circuit without the anode and cathode electrodes. One percent of hydrogen in helium was used as a reacting sweep gas. These conditions were not the same as our present system, which was operated under closed circuit with or without applied potential with LSM as the cathode and LaAlO as the anode catalyst.

3.1.2. A model for the oxygen permeation through the LSM/YSZ/LaAlO

In this study, an oxygen permeation model through the LSM/YSZ/LaAlO fuel cell type reaction system with closed circuit and applied potential is proposed. Schematic models of oxygen permeation are shown in Fig. 3. The circuit was closed to allow the electron transfer. Two kinds of carrier gas were used: i.e. helium (Fig. 3(a)) and methane (Fig. 3(b)).

In the case of helium feed without applied potential, Fig. 3(a) shows general reaction paths as follows: (1) electrochemical reduction at the LSM surface to form oxygen ions, (2) incorporation of oxygen ions into the YSZ lattice, (3) recombination and desorption of oxygen ions to form oxygen molecules at the LaAlO anode.

The permeation of oxygen through an electrochemical media depends upon ionic conductivity (σ_i) and electronic conductivity (σ_e) of the media. Assuming surface concentration of oxygen ions is equilibrated with gas phase, they can be estimated from the following equations [21].

$$J_{O_2} = \frac{\text{Per, } O_2}{L} \ln\left(\frac{P_{\text{rich}}}{P_{\text{lean}}}\right) \tag{4}$$

$$\text{Per, } O_2 = \frac{R_g T}{16F^2} \frac{\sigma_i \sigma_e}{\sigma_i + \sigma_e} \tag{5}$$

$$\sigma_j = \left(\frac{A_j}{T}\right) \exp\left(\frac{-E_j}{R_g T}\right); \quad j = \text{i,e} \tag{6}$$

The ionic conductivities of LSM ($\sigma_{\text{i-LSM}}$) [22], the electronic conductivities of LSM ($\sigma_{\text{e-LSM}}$) [23,24], the ionic conductivities of YSZ ($\sigma_{\text{i-YSZ}}$) [25] and the electronic conductivities of YSZ ($\sigma_{\text{e-YSZ}}$) [26] were cited from the literatures and the values are summarized in Table 1.

However, these values of LaAlO are not available in the literature. Due to the recombination and desorption of oxygen ions to form oxygen molecules at the LaAlO anode, the overall rate of these processes at LaAlO might be estimated

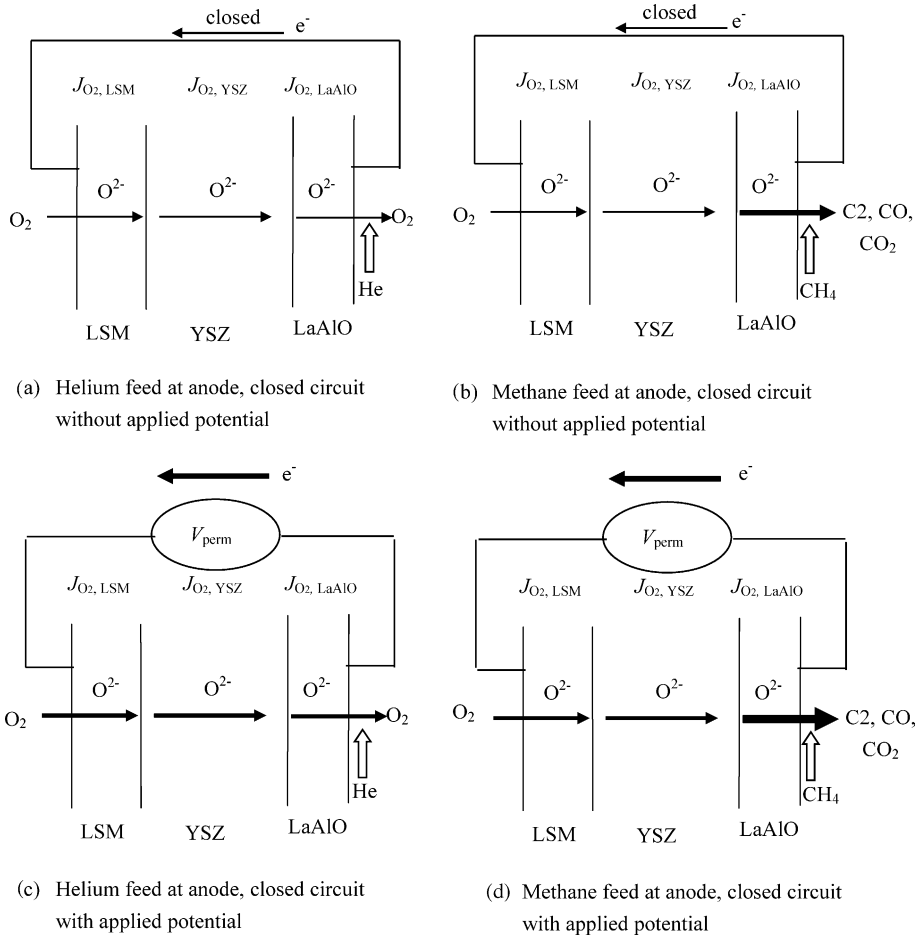

(a) Helium feed at anode, closed circuit without applied potential

(b) Methane feed at anode, closed circuit without applied potential

(c) Helium feed at anode, closed circuit with applied potential

(d) Methane feed at anode, closed circuit with applied potential

Fig. 3. Proposed schemes for oxygen permeation through LSM/YSZ/LaAlO under various conditions.

Table 1
Values of parameters for the calculations of oxygen permeation flux

Parameters	A_j (S K m^{-1})	E_j (kJ mol^{-1})	Reference
$\sigma_{\text{i-LSM}}$ (S m^{-1})	2.311×10^{11}	284	[22][a]
$\sigma_{\text{e-LSM}}$ (S m^{-1})	8.855×10^{7}	9	[23][b], [24][c]
$\sigma_{\text{i-YSZ}}$ (S m^{-1})	7.121×10^{7}	88	[25]
$\sigma_{\text{e-YSZ}}$ (S m^{-1})	9.244×10^{5}	87.5	[26]

$L_{\text{LSM}} = 1 \times 10^{-6}$ m, $L_{\text{YSZ}} = 1.5 \times 10^{-3}$ m, $L_{\text{LaAlO}} = 5 \times 10^{-6}$ m.
[a] At 1173 K, the value was interpolated between $La_{0.95}Sr_{0.05}MnO_3$ and $La_{0.8}Sr_{0.2}MnO_3$, and at 1273 K between $La_{0.9}Sr_{0.1}MnO_3$ and $La_{0.8}Sr_{0.2}MnO_3$.
[b] $\sigma_{\text{e-LSM}}$ was given at 1173 K.
[c] The activation energy was shown in the table.

from Eq. (7)

$$J_{O_2} = k_{O_2\text{-perm}} \ln\left(\frac{P_{\text{rich}}}{P_{\text{lean}}}\right) \tag{7}$$

where P_{rich} and P_{lean} represent partial pressure of oxygen at the rich and lean sides of LaAlO, respectively.

When the permeation is at steady-state, the oxygen permeation flux across different parts of the cell is equal to the observed experimental results.

$$J_{O_2,\text{Exp}} = J_{O_2,\text{LSM}} = J_{O_2,\text{YSZ}} = J_{O_2,\text{LaAlO}} \tag{8}$$

The values of $k_{O_2\text{-perm}}$ of LaAlO at different temperatures were determined by using an all-purpose equation solver, EQUATRAN-G (Omega Simulation, Japan). P_{rich} of LSM is partial pressure of oxygen at the feed side (101.3 kPa) while P_{lean} of LaAlO is partial pressure of oxygen at the permeate side, which are calculated from the experiments. The estimated $k_{O_2\text{-perm}}$ value was shown as follows.

$$k_{O_2\text{-perm}} = 0.413 \exp\left(\frac{-170400}{R_g T}\right) \tag{9}$$

In the case of methane feed without applied potential, oxygen ions directly reacted with methane at the anode (Fig. 3(b)). It was expected that the oxygen permeation rate could be enhanced. Due to the chemical reaction at the anode catalyst surface, the overall reaction rate could depend on partial pressure of methane and surface oxygen concentration. The oxygen surface reaction coefficient ($k_{O_2\text{-Rxn}}$) was estimated from experimental oxygen permeation flux by the following equation.

$$J_{O_2} = k_{O_2\text{-Rxn}} P_{CH_4} \ln\left(\frac{P_{\text{rich}}}{P_{\text{lean}}}\right) \tag{10}$$

No oxygen was observed in gas phase of the permeate side due to reactions with methane. The surface oxygen may not be in the equilibrium with oxygen in gas phase. However, the surface oxygen concentration in methane feed could be assumed similar to the helium case. Therefore, P_{lean} in the helium case was used in Eq. (10)

In the case of closed circuit with applied potential, it was expected that the oxygen transfer could be accelerated with increasing applied potential (in Fig. 3(c and d)). Linear relationship between applied potential and oxygen permeation flux was assumed and the following equation could be proposed.

$$J_{O_2} = J_{O_2,0V} + k_V V_{\text{Per}} \tag{11}$$

The values of $J_{O_2,0V}$ without applied potential can be calculated by Eqs. (4)–(6) and (7) for the helium feed case and by Eqs. (4)–(6) and (10) for the methane feed case, respectively.

3.2. Steady-state oxygen permeation results

3.2.1. Helium feed

Fig. 4 shows the effect of the applied potential on the oxygen flux at various temperatures. Linear relationships between the oxygen permeation flux and the applied potential were observed for all different temperatures. As shown in Fig. 4, the oxygen could be permeated without applied potential due to the system possessed an internal "concentration cell" potential as a driving force. For example, the concentration cell potential is 0.225 V at 1223 K. This value agrees well with OCV value calculated from Nernst equation.

$$E = \frac{R_g T}{4F} \ln\left(\frac{P_{\text{feed}}}{P_{\text{perm}}}\right) \tag{12}$$

Therefore, we can assume surface oxygen concentration at the lean side of LaAlO is in equilibrium with oxygen in gas phase at the permeate side.

The proportional constants (k_V) from Eq. (11) could be determined from the slopes and expressed as Eq. (13).

$$k_{V,\text{He}} = 0.102 \exp\left(\frac{-122700}{R_g T}\right) \tag{13}$$

Fig. 5 shows the plots between $\ln(J_{O_2})$ and $1000/T$ at different levels of the applied potential. The solid lines represent the results calculated from Eqs. (4)–(7), (11) and (13). The oxygen flux increases with the increasing temperature and applied potential.

The solid lines in Fig. 5, can be approximated by straight lines of Arrhenius' plots by Eq. (14).

$$J_{O_2} = A_{\text{Per}} \exp\left(\frac{-E_{\text{Per}}}{R_g T}\right) \tag{14}$$

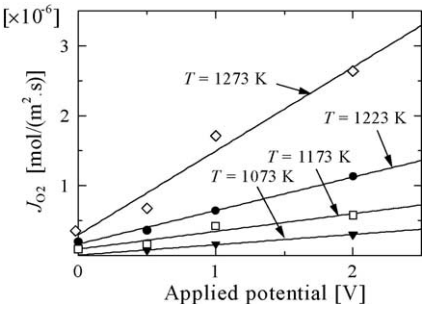

Fig. 4. Effect of applied potential on oxygen flux at various temperatures by steady-state permeation experiments using helium feed at anode side.

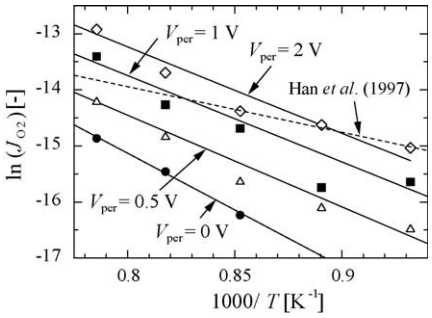

Fig. 5. Arrhenius' plot between ln(J_{O_2}) and 1000/T at different levels of applied potential by steady-state permeation experiments using helium feed at anode side.

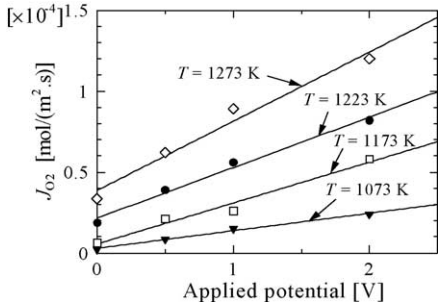

Fig. 6. Effect of applied potential on oxygen flux at various temperatures by steady-state permeation experiments using methane feed at anode side.

The overall activation energy of the oxygen transport through the cell (E_{Per}) was calculated from the slopes and the results are shown in Table 2. The activation energy is decreased from 170 kJ/mol in case of closed circuit with no applied potential to 119 kJ/mol with applied potential is 2 V. TPD experiments have shown that the applied potential also decreased the activation energy of the oxygen desorption from 140 kJ/mol to 93 kJ/mol when applied potential 2 V [19]. Comparing these values, the activation energies of oxygen permeation are close to the activation energies of oxygen desorption.

The dashed line in Fig. 5 shows the results calculated from Han's model [9]. The comparison of our model with Han's model will be described later (Section 3.2.4).

3.2.2. Methane feed

Instead of helium, methane was fed to the anode chamber to react with the permeating oxygen. At 1273 K, the electromotive force from the experiment is 1.09 V, which is near to the theoretical value of ethylene formation (1.05 V). Linear relationships between the oxygen permeation flux and the applied potential were observed for all different temperatures as shown in Fig. 6. The proportional constants (k_V) from Eq. (11) could be determined from the slopes and the expression is shown in Eq. (15).

$$k_{V,CH_4} = 0.875 \exp\left(\frac{-104150}{R_g T}\right) \quad (15)$$

Fig. 7 shows the plots between ln(J_{O_2}) and 1000/T at different levels of the applied potential. The oxygen flux with the methane feed was estimated from the equivalent rate of oxygen required for the oxidation reaction. The oxygen surface reaction coefficient ($k_{O_2\text{-Rxn}}$) estimated from the experimental oxygen permeation flux by using Eq. (8) was shown as follows.

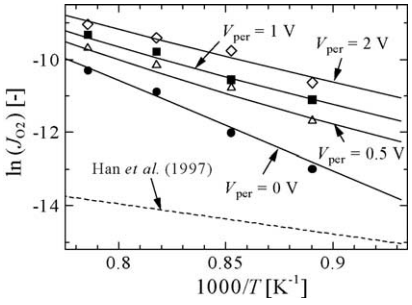

Fig. 7. Arrhenius' plot between ln(J_{O_2}) and 1000/T at different levels of applied potential by steady-state permeation experiments using methane feed at anode side.

$$k_{O_2\text{-Rxn}} = 8.577 \times 10^{-3} \exp\left(\frac{-195100}{R_g T}\right) \quad (16)$$

The solid line with V_{Per} = 0 V represents the calculated results by Eqs. (4)–(6), (10) and (16). The solid lines for V_{Per} = 0.5 V, 1 V and 2 V were calculated by Eqs. (4)–(6), (10), (11) and (15), (16).

The solid lines in Fig. 7 can be approximated by straight lines of Arrhenius' plots by Eq. (14). The overall activation energy of the oxygen transport through the cell (E_{Per}) was calculated from the slopes and the results are shown in Table 3. The applied potential increases the oxygen flux and also decreases the activation energy of the oxygen transport.

Compared with the helium feed case, the oxygen flux is significantly improved when methane is fed to the anode side. The oxygen permeation fluxes under the methane feed are 1–2

Table 2
Summary of the values of pre-exponential factors of oxygen permeation and activation energy at different levels of applied potential from steady-state permeation results using helium feed at anode side

V_{Per} (V)	A_{Per} (mol m^{-2} s^{-1})	E_{Per} (kJ mol^{-1})
0	3.499	170
0.5	1.280	154
1	0.675	144
2	0.157	119

Table 3
Summary of the values of pre-exponential factors of oxygen permeation and activation energy at different levels of applied potential from steady-state permeation results using methane feed at anode side

V_{Per} (V)	A_{Per} (mol m^{-2} s^{-1})	E_{Per} (kJ mol^{-1})
0	3.632×10^4	219
0.5	186.9	157
1	82.84	145
2	15.77	124

orders of magnitude higher than those under the helium feed. It is clear that the reaction of methane with the permeated oxygen at the anode catalyst significantly improves the overall oxygen permeation flux due to the surface oxygen kinetics with methane. The dashed line in Fig. 7 represents the Han's model.

3.2.3. Oxygen partial pressure profiles and permeation mechanism

Fig. 8 shows the oxygen partial pressure profile from the simulation results at 1223 K. In the case of the helium feed (solid line), it is obvious that the major oxygen permeation resistance through the cell or the rate-limiting step of this system is at the LaAlO electrode. Although the thickness of YSZ electrolyte is much more than the electrodes, the resistance of YSZ electrolyte is negligible. With the methane feed case (dashed lines), the resistances of three steps are comparable; consequently, the rate steps at the cathode and the electrolyte need to be taken into account.

In the case without methane, oxygen ions release electrons and recombine into oxygen molecules, which are then desorbed into the gas phase. On the other hand, with the methane feed, oxygen ions could directly react with methane to form CO_2, CO and C_2 hydrocarbons.

Mechanisms of the oxygen activation on the LSM and the bulk transport of O^{2-} in YSZ might be the same as the helium feed case as shown in the previous sections. The change in the surface reaction step on the anode from the recombination and desorption of oxygen ion to the reaction of oxygen species with methane would be the main reason for the increase of oxygen flux for the methane feed.

3.2.4. Effect of YSZ thickness

The effect of YSZ thickness on the oxygen permeation flux is simulated and the results are shown in Fig. 9. In the case of helium feed, the oxygen permeation flux is independent on the YSZ thickness as noted in the previous section that LaAlO is the rate-limiting step. However, in the case of methane feed, the resistance of YSZ electrolyte is comparable to that of LaAlO. The rate of oxygen permeation depends on the YSZ electrolyte. The flux increases with decreasing the thickness of YSZ electrolyte membrane. However, for YSZ with thickness below 10 μm, there is no significant improvement on the oxygen flux. The tendency is the same for $T = 1223$ K and 1273 K.

3.2.5. Estimation of oxygen permeation from a model proposed by Han et al. [9]

Han et al. [9] proposed Eqs. (1)–(3) for the permeation of oxygen through YSZ membrane but their system was tested under unusual conditions; i.e. very thin YSZ membrane of 2–15 μm, low oxygen partial pressure in an oxygen source chamber of 5.33 kPa and without external circuit (open circuit). Dashed lines in Figs. 5 and 7 show the oxygen permeation flux calculated from Eqs. (1)–(3) using a YSZ with thickness of 1.5 mm. The estimated oxygen flux is much larger than that of the helium feed (compared with $V_{Per} = 0$ in Fig. 5) and far less than that of the methane feed (compared with $V_{Per} = 0$ in Fig. 7). This tendency can be understood by considering that the sweep gas of the permeate side contained 1% of hydrogen in their experiments [9].

Hydrogen in the sweep gas caused the promotion of the oxygen permeation by the surface reaction but the partial pressure was too low to complete the enhancement of the oxygen permeation. When hydrogen was mixed in the sweep gas, an electromotive force of about 1 V should be generated between the two electrodes. This may be the reason of the agreement with the plot of $V_{Per} = 1$ V in Fig. 5.

The differences in the activation energy should be caused by the differences in the surface reaction on the anode material. Further studies are required to find more details.

All these results show that it is essential for the model of the SOFC-type reactor to include the permeation of oxygen through the cathode, the electrolyte and the anode.

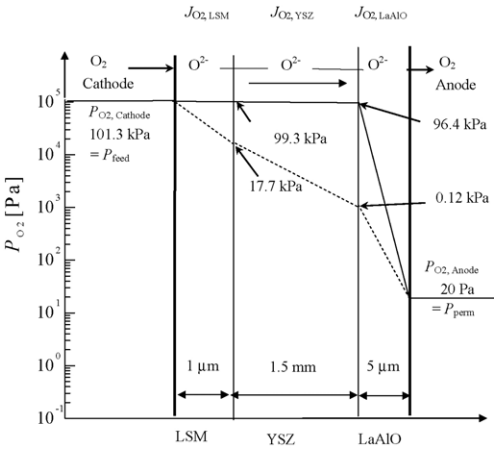

Fig. 8. The mechanism of oxygen permeation and the profile of oxygen partial pressure in LSM/YSY/LaAlO from the simulation results at 1223 K (solid line: helium feed, dashed line: methane feed).

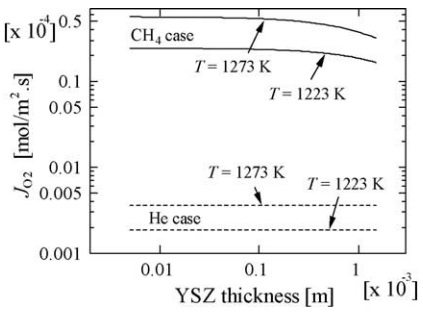

Fig. 9. Effect of YSZ thickness on oxygen permeation in helium and methane case.

4. Conclusion

The oxygen transport through the LSM/YSZ/LaAlO SOFC-type reactor was studied at various operating conditions. The oxygen permeation flux was 8.90×10^{-8} mol m^{-2} s^{-1} at 1173 K with an activation energy of 170 kJ mol^{-1}. Increasing the applied potential increased the oxygen permeation fluxes by one order of magnitude and reduced the activation energy of the oxygen permeation. The oxygen permeation fluxes under the methane feed are 1–2 orders of magnitude higher than those under the helium feed. A model of oxygen permeation was proposed. In the helium case, the oxygen permeation at the LaAlO anode was the rate-limiting step for the oxygen permeation. However, by changing helium to reactant gas as methane, the resistances in the three parts (LSM/YSZ/LaAlO) become comparable.

Acknowledgements

The authors gratefully acknowledged the financial support from the Thailand Research Fund (TRF) and TJTTP-JBIC. A part of this study was also supported by a Grant-in-aid for Scientific Research, from the Ministry of Education, Culture, Sports, Science and Technology of Japan (MEXT).

References

[1] B.C.H. Steele, J. Mater. Sci 36 (2001) 1053–1068.
[2] O. Yamamoto, Electrochim. Acta 45 (2000) 2423–2435.
[3] K.K. Moe, T. Tagawa, S. Goto, J. Ceram. Soc. Jpn. 106 (1998) 242–247.
[4] K.K. Moe, T. Tagawa, S. Goto, J. Ceram. Soc. Jpn. 106 (1998) 754–758.
[5] A.S. Carrillo, T. Tagawa, S. Goto, Mater. Res. Bull. 36 (2001) 1017–1027.
[6] T. Tagawa, K.K. Moe, T. Hiramatsu, S. Goto, Solid State Ionics 106 (1998) 227–235.
[7] T. Tagawa, K.K. Moe, M. Ito, S. Goto, Chem. Eng. Sci. 54 (1999) 1553–1557.
[8] T. Tagawa, K. Kuroyanagi, S. Goto, S. Assabumrungrat, P. Praserthdam, Chem. Eng. J. 93 (2003) 3–9.
[9] J. Han, G. Xomeritakis, Y.S. Lin, Solid State Ionics 93 (1997) 263–272.
[10] Y. Nigara, J. Mizusaki, M. Ishigame, Solid State Ionics 79 (1995) 208–211.
[11] Y. Teraoka, Y. Honbe, J. Ishii, H. Furukawa, I. Moriguchi, Solid State Ionics 152–153 (2002) 681–687.
[12] S. Lee, K.S. Lee, S.K. Woo, J.W. Kim, T. Ishihara, D.K. Kim, Solid State Ionics 158 (2003) 287–296.
[13] C.E. Platon, W.J. Thomson, Ind. Eng. Chem. Res. 41 (2002) 6637–6641.
[14] F.T. Akin, Y.S. Lin, Y. Zeng, Ind. Eng. Chem. Res. 40 (2001) 5908–5916.
[15] Z. Shao, G. Xiong, Y. Cong, W. Yang, J. Membr. Sci. 164 (2000) 167–176.
[16] J. Tong, W. Yang, B. Zhu, R. Cai, J. Membr. Sci. 203 (2002) 175–189.
[17] T. Ishihara, Y. Tsuruta, T. Todaka, H. Nishiguchi, Y. Takita, Solid State Ionics 152–153 (2002) 709–714.
[18] Y. Zeng, Y.S. Lin, J. Catal. 193 (2000) 58–64.
[19] W. Kiatkittipong, T. Tagawa, S. Goto, S. Assabumrungrat, P. Praserthdam, Solid State Ionics 166 (2004) 127–136.
[20] S. Goto, T. Tagawa, S. Assabumrungrat, P. Praserthdam, Catal. Today 82 (2003) 223–232.
[21] V.V. Kharton, A.V. Kovalevsky, A.P. Viskup, F.M. Figueiredo, J.R. Frade, A.A. Yaremchenko, E.N. Naumovich, Solid State Ionics 128 (2000) 117–130.
[22] I. Yasuda, K. Ogasawara, M. Hishinuma, T. Kawada, M. Dokiya, Solid State Ionics 86–88 (1996) 1197–1201.
[23] Z. Li, M. Behruzi, L. Fuerst, D. Stovet, in: S.C. Singhal, H. Iwahara (Eds.), SOFC-III, PV 93-4, The Electrochemical Society, Pennington, NJ, 1993, p. 171.
[24] V.V. Kharton, A.P. Viskup, I.P. Marozau, E.N. Naumocich, Mater. Lett. 57 (2003) 3017–3021.
[25] S.P.S. Badwal, Solid State Ionics 52 (1992) 23–32.
[26] C. Xia, S. Zha, W. Yang, R. Peng, D. Peng, G. Meng, Solid State Ionics 133 (2000) 287–297.